Electronic Supplementary Information for Journal of Materials Chemistry A

Controllable growth of graphene/Cu composite and its nanoarchitecture-dependent electrocatalytic activity to hydrazine oxidation

Chengbin Liu,*[a] Hang Zhang,[a] Yanhong Tang,[b] and Shenglian Luo*[a]

[a] State Key Laboratory of Chemo/Biosensing and Chemometrics, Hunan University, Changsha 410082, P. R. China. E-mail: chem_cbliu@hnu.edu.cn; sllou@hnu.edu.cn

[b] College of Materials Science and Engineering, Hunan University, Changsha 410082, P. R. China

1. Raman and X-photoelectron spectra

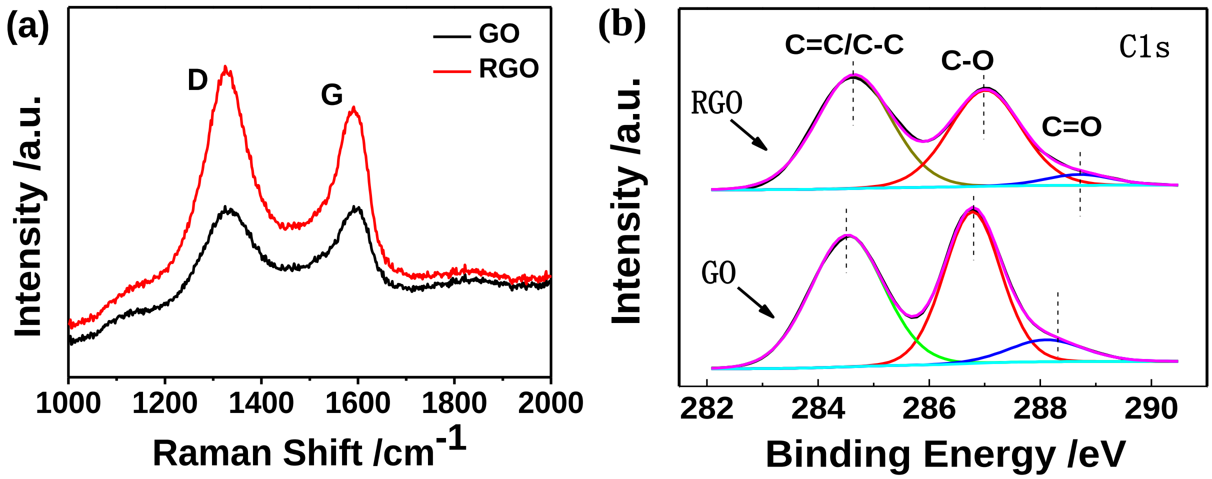

Fig. S1 (a) Raman spectra of GO and RGO. (b) High-resolution XPS C1s peak of GO and RGO. The Raman spectra of GO and RGO show characteristic D and G bands, where the D/G intensity ratio increases in RGO (1.349) relative to GO (0.998). Such increasing is often considered as a sign of GO reduction occurring, which is mainly because the number of smaller graphitic domains increase after reduction of GO. XPS confirms the reduction of GO based on the decreasing oxygen content in RGO, as evidenced by the dominant C=C/C–C peak at 284.5 eV for the RGO sample.

2. SEM images of RGO/Cu composite grown in various deposition cycles

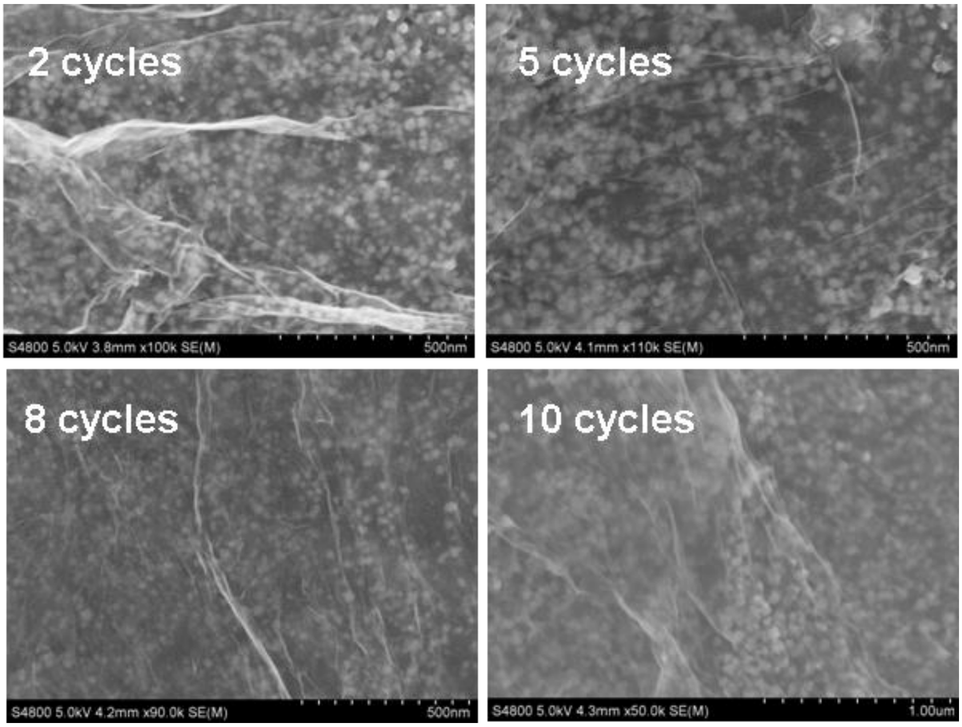

Fig. S2 SEM images for RGO/Cu composite prepared from 1 mM [Cu^{2+}] and 0.3 g L^{-1} GO using different cycle numbers for electrodeposition. It is found that the RGO is always the topmost layer irrespective of the cycle numbers.

3. CV electrolysis of GO or Cu-EDTA

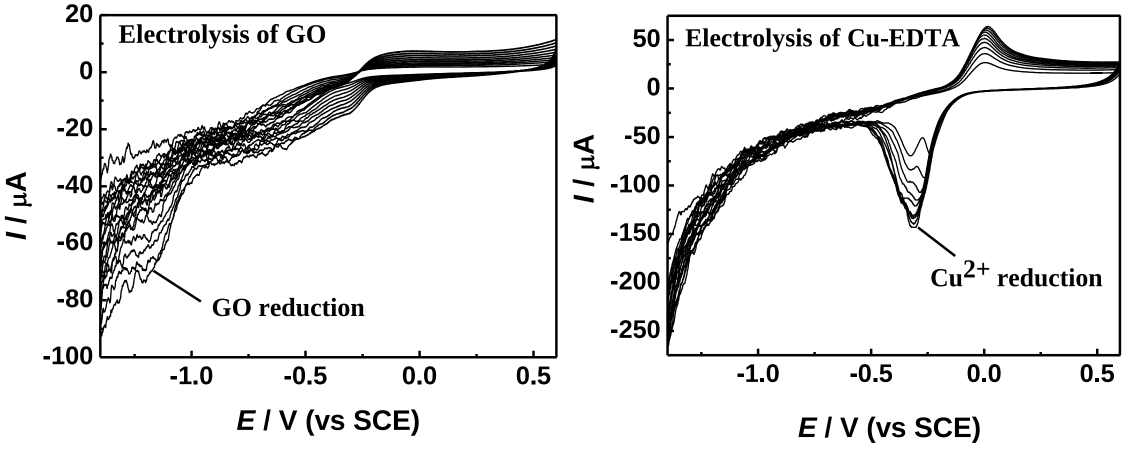

Fig. S3 CV electrolysis curves of 0.3 g L^{-1} GO (left) and 1 mM Cu-EDTA (right) in 0.067 M pH8 phosphate buffer solution for 10 cycles. It is found that the reduction peak potentials of GO and Cu^{2+} are –1.2[1,2] and –0.3 V (versus saturated calomel electrode (SCE)), respectively.

4. XPS measurements

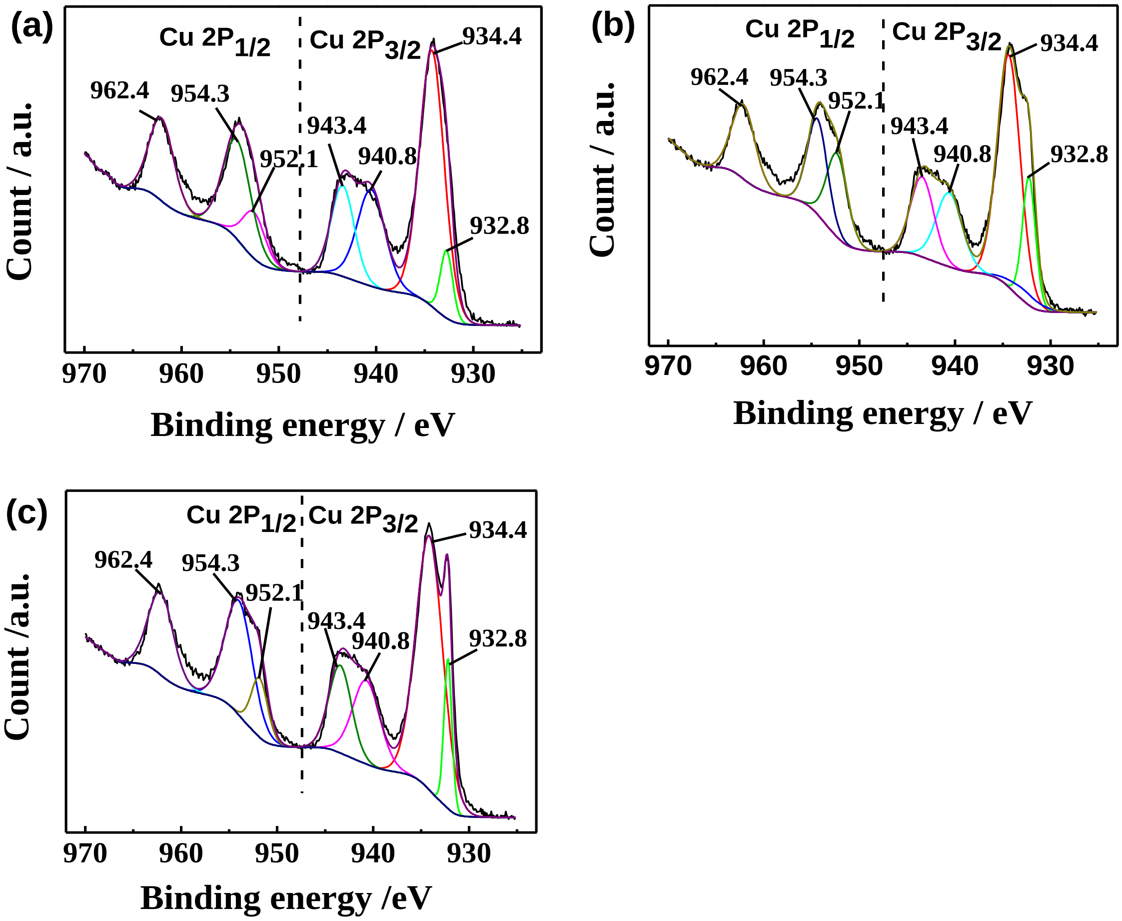

Fig. S4 XPS for (a) L-RGO/Cu, (b) S-RGO/Cu, and (c) H-RGO/Cu. Similar features are observed for the three composites. The peaks at 932.8 and 952.1 eV are ascribed to the Cu $2P_{3/2}$ and Cu $2P_{1/2}$ signals of metallic copper or Cu_2O (it is difficult to distinguish metallic copper and Cu_2O by XPS features of Cu 2P due to their very closed binding energies), respectively, and the peaks at 934.4 and 954.3 eV are ascribed to the Cu $2P_{3/2}$ and Cu $2P_{1/2}$ of CuO, respectively.[3–5]The other peaks located at higher binding energies (940–945 eV and 954–965 eV) can be attributed to satellite peaks characteristic of CuO.[6]

5. Cyclic voltammograms of bare GCE and RGO/GCE in $K_3[Fe(CN)_6]$

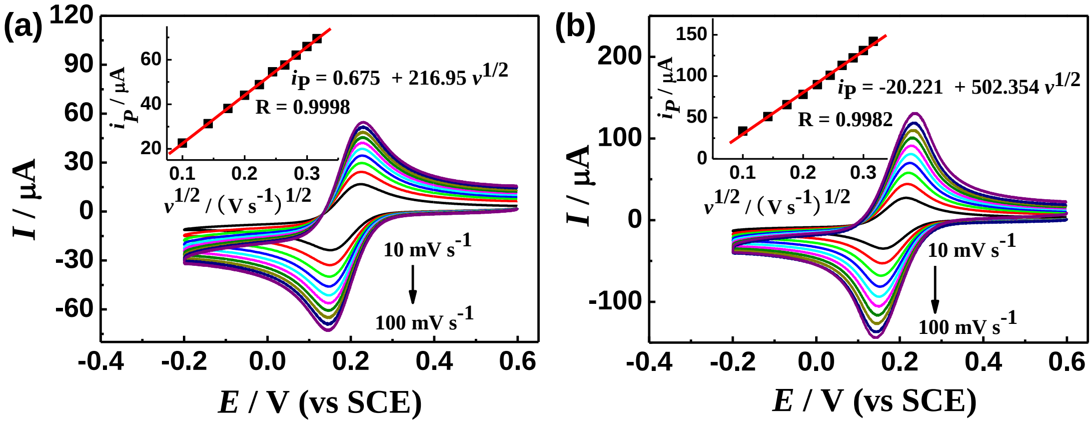

Fig. S5 Cyclic voltammograms at (a) the bare GCE and (b) the RGO/GCE in 0.1 M KCl containing 5 mM $K_3[Fe(CN)_6]$ at different scan rates (*v*) of 10, 20, 30, 40, 50, 60, 70, 80, 90, 100 mV s^{-1}. Insets are the plots of anodic i_p versus $\nu^{1/2}$.

6. Cyclic voltammograms for the electrodes in the back-ground electrolyte KOH

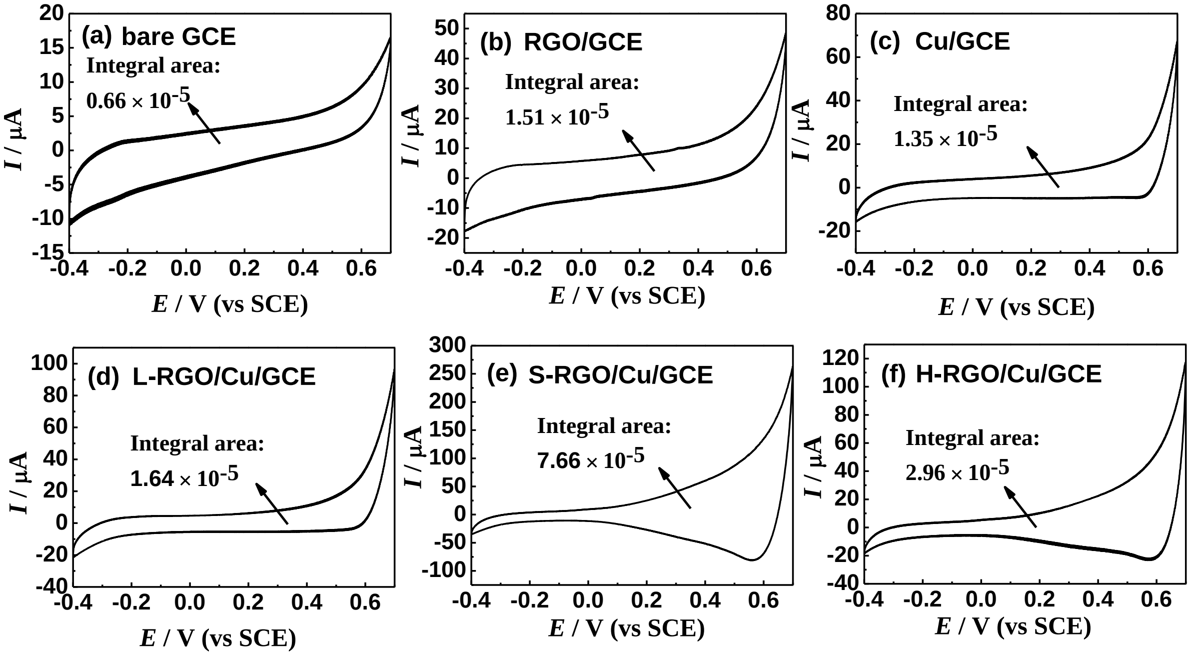

Fig. S6 Cyclic voltammograms for (a) bare GCE, (b) RGO/GCE, (c) Cu/GCE, (d) L-RGO/Cu/GCE, (e) S-RGO/Cu/GCE, and (f) H-RGO/Cu/GCE in 0.1 M KOH without N_2H_4 at the scan rate of 0.1 V s^{-1} in the potential range of –0.4–+0.7 V, with the corresponding integral area ($\int I dV$) presented.

7. The effect of scan rate investigated on the RGO and the Cu electrodes

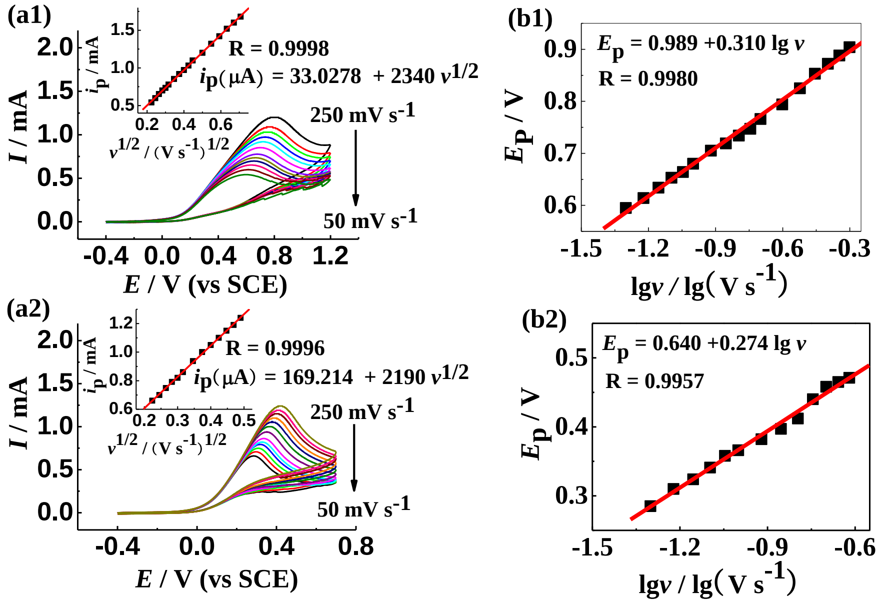

Fig. S7 Cyclic voltammograms at the GCEs loaded with (a1) RGO and (a2) Cu nanoparticles in 0.1 M KOH containing 10 mM hydrazine at various scan rates of 50, 60, 70, 80, 90, 100, 120, 140, 160, 180, 200, and 250 mV s^{-1}. Insets represent the dependence of the peak current on the square root of the scan rate. (b1) and (b2) represent the dependence of the peak potential in (a1) and (a2), respectively, on the natural logarithm of the scan rate.

8. Stability test of the electrodes using cyclic voltammetry

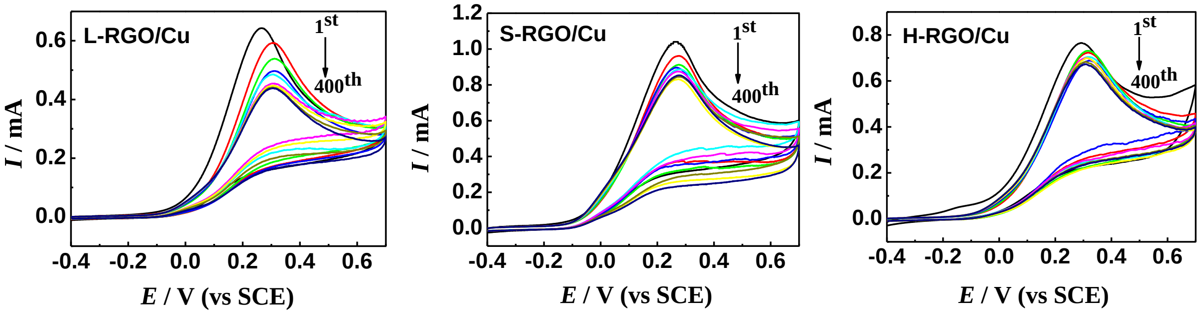

Fig. S8 Cyclic voltammograms for the L-, S-, and H-RGO/Cu composite electrodes in the potential range of −0.4−+0.7 V at the scan rate of 100 mV s^{-1} in 0.1 M KOH solution containing 10 mM N_2H_4. The 1st, 50th, 100th, 150th, 200th, 250th, 300th, 350th, 400th cycles were demonstrated.

References

1. L. Y. Chen, Y. H. Tang, K. Wang, C. B. Liu and S. L. Luo, *Electrochem. Commun.*, 2011, **13**, 133.
2. C. B. Liu, Y. R. Teng, R. H. Liu, S. L. Luo, Y. H. Tang, L. Y. Chen and Q. Cai, *Carbon*, 2011, **49**, 5312.
3. L. Martin, H. Martinez, D. Poinot, B. Pecquenard and F. Le Cras, *J. Phys. Chem. C*, 2013, **117**, 4421.
4. S. Gonzalez, M. Perez, M. Barrera, A. R. G. Elipe and R. M. Souto, *J. Phys. Chem. C*, 1998, **102**, 5483.
5. H. C. Gao, Y. X. Wang, F. Xiao, C. B. Ching and H. W. Duan, *J. Phys. Chem. C*, 2012, **116**, 7719.
6. G. A. Gelves, Z. T. M. Murakami, M. J. Krantz and J. A. Haber, *J. Mater. Chem.*, 2006, **16**, 3075.